Chemical Engineering Journal 499 (2024) 155942

Contents lists available at ScienceDirect

Chemical Engineering Journal

journal homepage: www.elsevier.com/locate/cej

Coordination, hydration, and diffusion of vanadyl cations in negatively charged polymer membranes

José C. Díaz [a,1], Christina E. Uhlenbrock [a,1], Nirala Singh [a,*], Jovan Kamcev [a,b,*]

[a] Department of Chemical Engineering, University of Michigan, North Campus Research Complex B28, 2800 Plymouth Rd., Ann Arbor, MI 48109, USA
[b] Macromolecular Science and Engineering, University of Michigan, North Campus Research Complex B28, 2800 Plymouth Rd., Ann Arbor, MI 48109, USA

ARTICLE INFO

Keywords:
Ion-exchange membrane
X-ray absorption spectroscopy
Ion hydration
Ion diffusion

ABSTRACT

Charged polymer membranes that selectively transport ions are crucial for advancing electrochemical technologies for water purification, resource recovery, and energy generation/storage. Recent studies suggest that the ion selectivity trends of such membranes are due to ion dehydration at the membrane/solution interface, where ions that require less energy to shed their hydration can partition more favorably into the membrane. However, direct evidence of ion dehydration in polymer membranes at relevant conditions is scarce, with claims based primarily on correlations between ion hydration energies and membrane transport properties. This study investigates the electronic environment, local coordination, and hydration of vanadyl counter-ion in negatively charged membranes with broadly varying water content via x-ray absorption spectroscopy. The results highlight that vanadyl counter-ions maintain similar oxidation state, electronic state, and coordination number in the membranes as in aqueous solutions of vanadyl sulfate and that vanadyl dehydration is unlikely in these membranes. However, as the membrane water content decreases, the vanadyl diffusion coefficient decreases and the activation energy of diffusion increases. We attribute these significant changes in membrane transport properties to increased Coulombic interactions between vanadyl and the fixed charge groups, resulting from a decreased dielectric constant of the membrane, rather than to ion dehydration at the membrane/solution interface. This study represents significant progress in understanding the mechanisms that govern ion transport in charged polymer membranes over a broad range of water content, highlighting the critical role of Coulombic interactions between the fixed charges and mobile ions.

1. Introduction and background

Electrochemical technologies for water purification, resource recovery, and energy generation/storage depend on ion-exchange membranes (IEMs) to regulate ion transport between electrodes [1–4]. The primary function of IEMs is to transport ions that are oppositely charged to the membrane (i.e., counter-ions), while restricting the transport of similarly charged ions (i.e., co-ions). Additionally, in certain applications, these membranes must effectively differentiate between different counter-ions [4,5]. For example, membranes with high selectivity for Li^+ ions in solutions containing other cations (i.e., Na^+ and Mg^{2+} in geothermal brines; Co^{2+} and Ni^{2+} in spent batteries leachate) can enable the efficient recovery of lithium salts, critical for rechargeable lithium ion batteries [4,6]. Similarly, membranes with high selectivity for H^+ over redox active vanadium cations can optimize the efficiency of vanadium redox flow batteries (VRFBs), thereby improving power and energy densities [7–9]. Consequently, there is an increasing need to develop IEMs with enhanced selectivity for counter-ions, aimed at bolstering resource recovery and energy storage applications [4,10]. Developing IEMs with tailored selectivity requires fundamental understanding of how factors such as polymer structure, the chemistry and concentration of fixed charged groups, and membrane water content influence counter-ion transport [4,11].

Ion transport in IEMs is driven by an electrochemical potential gradient across the membrane [12]. The transport mechanism involves the thermodynamic partitioning of ions from the solution into the membrane phase, followed by diffusion down the electrochemical potential gradient [4,13]. Consequently, the selectivity of IEMs for specific

* Corresponding authors at: Department of Chemical Engineering, University of Michigan, North Campus Research Complex B28, 2800 Plymouth Rd., Ann Arbor, MI 48109 USA.
E-mail addresses: snirala@umich.edu (N. Singh), jkamcev@umich.edu (J. Kamcev).
[1] Authors contributed equally to this work.

https://doi.org/10.1016/j.cej.2024.155942
Received 19 July 2024; Received in revised form 3 September 2024; Accepted 16 September 2024
Available online 18 September 2024

counter-ions depends on both the partitioning selectivity and the diffusion selectivity [13]. Recent studies have hypothesized ion dehydration within the membrane as a critical factor influencing selective ion partitioning and transport in IEMs (Fig. 1a), particularly for similarly charged ions [14]. That is, as ions enter the membrane, they shed part or all of their hydration shells. The difference in the ability of different ions to dehydrate, generally quantified by the Gibbs free energy of hydration, is proposed to result in an observed transport selectivity. For example, ions with larger ionic radii and lower hydration energies (e.g., Cs^+ or I^-) are more likely to partition into a membrane than those with smaller ionic radii and higher hydration energies (e.g., Li^+ or F^-) [14–16]. The occurrence of ion dehydration has also been invoked to explain ion selectivity in other membrane technologies, including nanofiltration (NF) and reverse osmosis [16–25]. The primary objective of this study is to investigate ion hydration in charged polymer membranes and rigorously test the hypothesis of ion dehydration.

Molecular dynamics (MD) simulations have provided evidence for ion dehydration in sub-nanometer rigid pores modeled by graphene sheets (*ca.* 2.5–6.5 Å), but the relevance of these results to polymer membrane systems is uncertain [24–26]. The rigid and uniform pores modeled in these simulations differ markedly from the structure of polymer membranes, which are generally amorphous and exhibit a broad range of free volume sizes that are difficult to determine experimentally, particularly in the subnanometer range. Furthermore, unlike the static pores of rigid inorganic materials, the polymer chains in these membranes are mobile, making the free volume in amorphous polymers a dynamic feature. MD simulations that more accurately represent the environment of polymer membranes suggest that ions often retain their first hydration shell when partitioning into the polymer phase, even for dense polymers with little swelling [27].

Much of the experimental evidence supporting ion dehydration in IEMs has been indirect. For example, ion dehydration is often invoked when correlations are found between the ion Gibbs free energy of hydration and either the membrane partitioning selectivity or ion activation energy of transport, assuming that the partitioning step is rate limiting [14]. More recently, liquid time-of-flight secondary ion beam mass spectrometry was used to investigate *in-situ* ion dehydration during transmembrane transport in polyamide NF membranes [16]. The authors observed a notable decrease in the average hydration number of sodium ions during their passage through various NF membranes, suggesting partial dehydration. However, a significant limitation of this approach is the reliance on ultrahigh vacuum conditions to facilitate water and ion transport across the membrane. Such conditions can substantially alter the hydration of the membrane at the interface at which the measurement is taking place, which would impact the availability of water molecules to hydrate the ions.

The structure of ions within membranes, including their hydration, can play a critical role in diffusion and the resulting diffusion selectivity. Counter-ions that dehydrate may be able to form various types of ion pairs with the fixed charged groups (Fig. 1b), which can subsequently impact ion diffusion. These ion pairs are typically classified as solvent-separated, solvent-shared, and contact ion pairs, in order of decreasing distance between charged species and decreasing hydration between them [28]. The formation and distribution of these ion pairs within membranes can be affected by the membrane water content [11,29,30]. The electrostatic attraction between ions that form ion pairs is greatly influenced by how easily water can solvate ions of different sizes and charge distributions [31]. For example, solvation can counteract the electrostatic penalty of bringing two like-charged ions together. Therefore, contact ion pairs must overcome stronger electrostatic interaction energies than solvent-shared and solvent-separated ion pairs during diffusion (Fig. 1c) [31,32]. Accurately characterizing counter-ion dehydration and understanding how membrane properties, such as water content, influence dehydration and the distribution of ion pairs within IEMs are critical for advancing our understanding of ion transport mechanisms in dense polymer membranes. Moreover, a fundamental understating of changes in ion hydration in different environments is crucial for the success of other applications relying on the full hydration of ions, such as hydrogels used for aqueous zinc batteries or superlubricity in hydration lubrication for tribological applications [33–35].

X-ray absorption fine structure (XAFS) is a non-destructive technique capable of identifying the element-specific local coordination of ions in solution [36–44]. The XAFS spectra are divided into near-edge (XANES) and extended (EXAFS) regions [43]. The XANES portion provides information about the electronic structure and oxidation states of ions and highlights differences in ion-ligand interactions [39,43]. The EXAFS portion yields the average coordination number around a central ion and the bond distances between ions and ligands [28,40,45,46]. While XAFS provides detailed information on the coordination of ions in solution, it has not been used extensively to investigate ion coordination in charged polymers, such as IEMs [46–59]. Several studies have investigated ion coordination and speciation in anion-exchange resins that are lightly crosslinked and have high water content [46,48,56–58]. Conversely, XAFS studies of cation-exchange membranes (CEMs) have primarily focused on understanding counter-ion coordination within Nafion and other CEMs [50–53,60]. While these studies have been pioneering in their *in-situ* exploration of ion coordination within IEMs, they have been limited in scope, focusing on a few membranes with minimal variations in properties such as equilibrium membrane water content, which is known to significantly affect counter-ion transport in IEMs [11,61]. This limitation restricts our ability to understand counter-

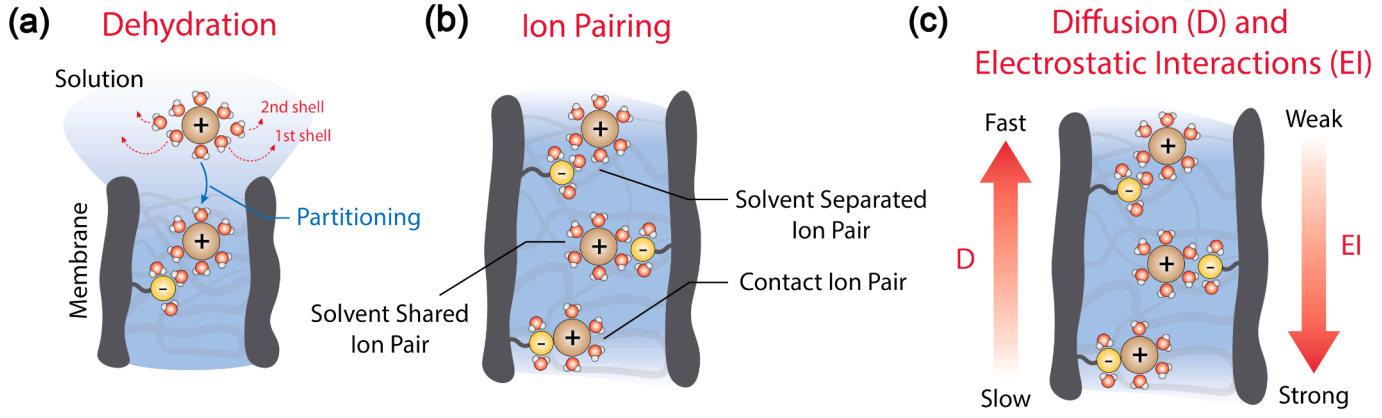

Fig. 1. Schematics of the factors that can affect ion transport across IEMs. (a) Counter-ion dehydration upon partitioning in the membrane. (b) Types of ion pairs between counter-ions and charged groups in the membrane. (c) Electrostatic interactions affect the diffusion of counter-ions since strong electrostatic interactions result in larger energy barriers for ion transport.

ion coordination and hydration *in situ* across different materials and ranges of membrane water content.

This study investigates the local coordination of vanadyl (VO^{2+}) counter-ions within negatively charged membranes with broadly varying water content via XAFS. We compared these findings with experimentally determined VO^{2+} diffusion coefficients and activation energies of diffusion. The experimental XANES spectra of VO^{2+} revealed that the electronic environment and oxidation state of VO^{2+} in all examined membranes are similar to those in an aqueous solution of $VOSO_4$. Furthermore, the EXAFS results demonstrated that the coordination number of VO^{2+} in the membranes does not differ substantially from that in an aqueous solution of $VOSO_4$, suggesting that VO^{2+} ions do not undergo dehydration to enter the membranes nor form contact-ion pairs with the fixed charge groups. However, VO^{2+} single diffusion coefficients decrease, and activation energies of diffusion increase as the membrane water content decreases. These notable changes in transport properties without a corresponding change in ion coordination are inconsistent with the hypothesis that ion dehydration is the primary factor influencing ion transport in IEMs. Specifically, Coulombic interactions between the counter-ions and fixed charge groups, and not counter-ion dehydration, adequately explain the observed diffusion trends. This study advances our fundamental understanding of the factors influencing counter-ion diffusion in negatively charged membranes, offering new insights into how membrane properties impact ion transport.

2. Results and discussion

2.1. Membrane properties

The primary objective of this study is to investigate the role of membrane water content on the hydration and diffusion of VO^{2+}counter-ions in negatively charged membranes. We synthesized six homogeneous cross-linked membranes with different water volume fractions and similar charge densities via free radical polymerization of a charged monomer and a cross-linker (see Sections S1 and S2 in the Supporting Information (SI) for materials and the synthesis procedure). To isolate and independently control the water content of the membranes, we tuned the amount of cross-linker and/or solvent in the pre-polymerization mixture, both of which affect the cross-link density of the membrane [11]. The charged monomer is 3-sulfopropyl methacrylate potassium salt (SPM), and the cross-linker is glycerol dimethacrylate (GDMA). The chemical structures of these monomers are shown in Fig. S1, and the composition of the six membranes are listed in Table S1. For comparison, we also studied Nafion 117, whose chemical structure is given in Fig. S2. This perfluorinated membrane is commonly used in vanadium redox flow batteries (VRFBs) and features a vastly different chemical environment relative to the aliphatic SPM-GDMA membranes [62]. The synthesized membranes are designated as SPM-GDMA(xx), where the xx represents the water volume percent in the vanadyl counter-ion form. We note the number 117 for Nafion 117 refers to a designation of the theoretical ion exchange capacity and the thickness of the Nafion membrane, not a water volume fraction. The measured water volume fraction of Nafion 117 is 0.442. The process to convert the as-synthesized membranes to the vanadyl counter-ion form is illustrated in Fig. S3, and images of the membranes in both forms are presented in Fig. S4.

Small angle x-ray scattering (SAXS) results of SPM-GDMA(33), SPM-GDMA(42), and SPM-GDMA(59) in the VO^{2+} form, presented in Fig. S5, support the homogeneity of these membranes since there are no features in the spectra (e.g., formation of sharp peaks) that indicate strong structural inhomogeneity. Conversely, the SAXS spectra of Nafion 117 in VO^{2+} form, presented in Fig. S5, exhibits a distinctive ionomer peak, characteristic of the hydrophilic phases within the membrane [63,64].

XAFS measurements were performed with the highest (SPM-GDMA (59)) and lowest (SPM-GDMA(33)) water content membranes to study the extremes. Table 1 lists the water volume fraction and charge density of these two membranes, while the properties for all other membranes involved in this study are compiled in Section S4 of the SI (Tables S2–S4 and Fig. S6). We also performed XAFS measurements with Nafion 117 membranes in the vanadyl counter-ion form.

2.2. Electronic environment and oxidation state of vanadyl within the membranes

Vanadium ions used in VRFBs can be investigated through x-ray absorption fine structure (XAFS) at the vanadium K-edge (5465 eV). This technique allows for precise identification and characterization of the electronic state and coordination environment of vanadium ions (see Fig. 2). As the oxidation state of vanadium increases, the K-edge shifts to higher energies, the pre-edge peak changes, and the white line (i.e., the post-edge peak) changes in shape and intensity. As a d-transition metal, vanadium exhibits a range of electronic states and coordination geometries that can be readily analyzed via XAFS. Moreover, XAFS measurements of vanadium species can be performed in transmission mode for membranes with thickness on the order of hundreds of micrometers, allowing *in situ* and potentially *in operando* analysis of both commercially and laboratory-prepared IEMs (Section S6). Among the four oxidation states of vanadium ions used in VRFBs, the vanadyl ion, VO^{2+}, is distinguished by its unique electronic structure and stable oxo-vanadium coordination complex. The coordination and electronic state of VO^{2+} within different media has been extensively studied [45]. Therefore, we focused on exploring the *in situ* coordination, hydration, and ion pair formation of vanadyl counter-ions in negatively charged membranes exhibiting a range of water content levels using XAFS to demonstrate the utility of this technique for investigating the local molecular environment around ions in IEMs.

A fundamental question addressed in this study is whether the oxidation and electronic states of vanadyl ions change when moving from an aqueous solution of vanadyl sulfate into negatively charged membranes. Both the pre-edge and the K-edge step of normalized μ(E) data for vanadium ions can be used to determine their oxidation state [66]. As depicted in Fig. 3a, the pre-edge and XANES of vanadyl in both solid and aqueous samples of vanadyl sulfate ($VOSO_4$) demonstrate similar edge locations and pre-edge peaks, confirming the vanadyl ions are in the 4+ oxidation state. While the oxidation state of vanadyl in the solid and aqueous $VOSO_4$ is the same, distinct differences in the μ(E) data are evident. Notably, a shoulder appears between 5470 eV and 5480 eV in the $VOSO_4$ solid data that is absent in the aqueous $VOSO_4$ results. Additionally there are distinct variations in the white line

Table 1
Equilibrium properties of membranes employed for XAFS measurements. Uncertainties represent the standard deviation of measurements performed on ten independent samples.

Membrane	Water Uptake (g(water)/g(dry polymer))	Water Volume Fraction (L(water)/ L(hydrated membrane))	Fixed Charge Density (L(water)/ L(hydrated membrane))	Ion Exchange Capacity (mmol/g(dry polymer))
SPM-GDMA(33)	0.344 ± 0.009	0.330 ± 0.008	1.55 ± 0.03	1.63 ± 0.04
SPM-GDMA(59)	0.984 ± 0.009	0.593 ± 0.008	1.56 ± 0.06	2.59 ± 0.08
Nafion 117	0.379 ± 0.005	0.442 ± 0.010	1.05 ± 0.10	0.902 ± 0.058

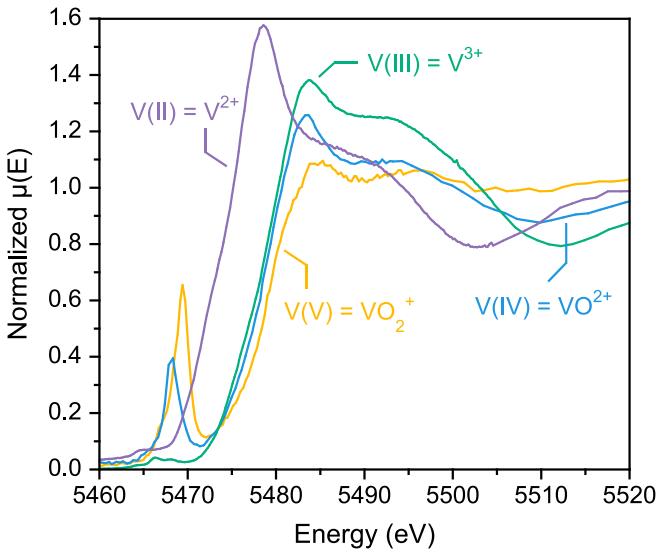

Fig. 2. Normalized XANES spectra of vanadium ions in aqueous solutions in all four oxidation states implemented in vanadium redox flow batteries, demonstrating the difference in the location of the pre-edge peak and edge peak with oxidation state. V(III) (0.2 M V, 0.7 M SO_4^{2-}) [65], V(IV) (0.3 M V, 0.3 M SO_4^{2-}), and V(V) (0.4 M V, 3 M SO_4^{2-}) samples are in sulfuric acid, V(II) (0.2 M V, 1 M ClO_4^-) sample is in perchloric acid [65].

intensity and shape (the peak around 5485 eV) between the solid and aqueous $VOSO_4$ samples. These discrepancies suggest changes in the electronic structure due to local ligand coordination differences between the two forms. The observed differences are not attributable to variation in oxidation states based on comparisons to the controls in Fig. 2. Instead, we attribute these differences to the coordination of vanadium by sulfate in solid $VOSO_4$, while in the aqueous $VOSO_4$, the vanadium dissociates as VO^{2+} and predominantly coordinates with water molecules, rather than with sulfate [45,67,68].

Fig. 3b and 3c demonstrate that both the pre-edge peak and edge location of vanadium in the CEMs are in the same location (5468.4 eV and 5483 eV, respectively) as those observed for aqueous $VOSO_4$. Furthermore, these spectral features correspond with the expected peak locations reported elsewhere [66]. These results suggest that the electronic structure of the vanadyl counter-ions in the membranes closely resembles that of vanadium ions in aqueous solutions, while distinctly differing from that of the solid salt form. To quantify this resemblance, we employed linear combination fitting using the ATHENA software, using both the solid and aqueous forms of $VOSO_4$ as reference standards [69]. The best fit for all three membrane samples was achieved with 100 % representation from aqueous $VOSO_4$ and 0 % from solid $VOSO_4$. This similarity in the XANES spectra between the membrane samples and aqueous vanadyl indicates a lack of coordination (i.e., contact ion pairing) between the sulfonate anions and vanadyl counter-ions in the membranes. Consequently, we propose that the vanadyl counter-ions in the membranes form either solvent-shared or solvent-separated ion pairs across the explored range of water contents.

We also investigated the oxidation and electronic states of vanadyl both in solution and in the membrane via UV–vis spectroscopy (Section S5). The sensitivity of UV–vis spectra to the bonding chemistry of transition metal ions, such as vanadyl, makes this technique particularly valuable for identifying coordination complexes, including contact ion pairs formed between anionic ligands and the vanadyl cation [68,70]. The spectra obtained for membranes with different water contents exhibit characteristic features similar to those of hydrated vanadyl ions in aqueous solutions of vanadyl sulfate and chloride (Fig. S7). Notably, the two prominent bands in the UV–vis spectra are associated with the tetragonal symmetry of the hydrated vanadyl ion, which includes the oxo-vanadium bond (V═O) and the equatorial water ligands [67,71–75]. These bands correspond to metal-to-ligand and ligand-to-metal charge transfer transitions, manifesting as absorption peaks at approximately 762 nm and 621 nm, respectively [71,75]. The primary peak positions and shapes in the spectra of dilute aqueous $VOSO_4$ solution, SPM-GDMA(33), SPM-GDMA(59), and Nafion 117 membranes closely align with established literature values for the solution-phase spectra of vanadyl ions, confirming the preservation of the electronic structure of vanadyl within the membrane. Notably, the lack of significant deviations in the UV–vis spectra of vanadyl within the membranes compared to those in aqueous solution corroborates the results from XANES spectroscopy, affirming the unaltered oxidation and electronic state of vanadyl ions within the membrane matrix.

2.3. Coordination and hydration of vanadyl within the membranes

Investigating counter-ion dehydration and ion pair formation in IEMs is challenging due to limitations in the spatial and temporal resolution required to capture *in situ* evidence of these phenomena within dense polymer membranes. EXAFS spectroscopy is a powerful tool for examining the local atomic arrangements surrounding the vanadyl counter-ion [45]. Specifically, EXAFS analysis enables the determination of coordination numbers, bond lengths, and coordination geometries of vanadyl ions in various chemical environments, including in solution and in membranes. The coordination number obtained by EXAFS refers to the number of water molecules in the immediate vicinity of an ion [45,76,77]. This metric is distinct from the ion hydration number, which quantifies the water molecules that accompany an ion as it executes a diffusion step [42,77,78]. While the coordination number

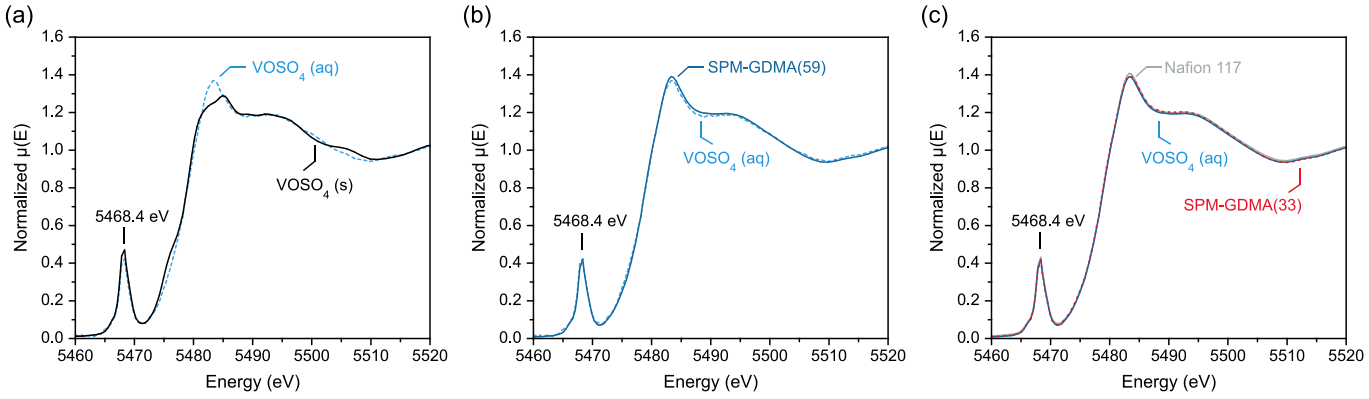

Fig. 3. (a) XANES spectra of the vanadium K-edge of solid (dried) $VOSO_4$ and 0.3 M aqueous solution of $VOSO_4$. (b) XANES spectra of the 0.3 M aqueous solution of $VOSO_4$ and vanadyl counter-ion in SPM-GDMA(59). (c) XANES spectra of vanadyl counter-ion in SPM-GDMA(33), SPM-GDMA(59), and Nafion 117. Slight changes in the peak shape at 5482 eV and the formation of a shoulder between 5470 eV and 5480 eV are indicative of changes between the $VOSO_4$ (s) and $VOSO_4$ (aq) samples.

provides an ensemble average reflecting the immediate surroundings of the ion, the hydration number offers a broader perspective on ion-water interactions, capturing the dynamic nature of hydration [42]. This distinction has been seldom made in previous discussions of ion dehydration in polymer membranes.

Previous studies have examined the coordination and electronic structure of the vanadyl ion in both the solid and solution states using electron paramagnetic resonance spectroscopy [73], density functional theory [73,76], nuclear magnetic resonance (NMR) spectroscopy [79,80], and XANES [45]. In aqueous solutions and at moderately low pH, vanadium (IV) typically exists as the pentahydrate vanadyl ion $[VO(H_2O)_5]^{2+}$ [68]. This ion exhibits an octahedral coordination geometry, with four water molecules occupying the equatorial plane and a fifth water molecule positioned axially opposite to the vanadium-oxo bond, albeit with a longer bond length than the equatorially coordinated waters [45,76,79,81]. Additionally, there is the possibility of weakly bound water molecules from the bulk solvent forming a second coordination sphere around the octahedral structure [68,79].

Fig. 4a shows the EXAFS magnitude plots of solid $VOSO_4$, a dilute aqueous solution of $VOSO_4$, and VO^{2+} in the SPM-GDMA(33) membrane. The primary differences between samples are in the intensity of the peak around 1.75 Å, which is higher in both the aqueous $VOSO_4$ and the membrane compared to the solid $VOSO_4$, and the feature around 2.5 Å that is more pronounced in the solid $VOSO_4$. The spectral data for SPM-GDMA(33) closely resembles that of the aqueous $VOSO_4$. The results are similar for the other membranes, as shown in Fig. 4b. These results indicate a similar local coordination structure for vanadyl in dilute aqueous solution and the three membranes, with a different structure evident for the solid $VOSO_4$ salt. To better understand the reasons for these structural differences, we fit the EXAFS data using the ARTEMIS software [69] and included the structural parameters from the fitting in Table S5 and fits in Figs. S8–S12.

For the solid $VOSO_4$ sample, we anticipated that, in addition to the double bonded oxygen group from the oxo-vanadium moiety, four oxygen atoms from the water ligands and another oxygen from the sulfate anion would be distinguished in the EXAFS fitting, as depicted in Fig. 4a. This fitting suggests a first shell dehydration and the formation of a contact ion pair between the vanadyl center and an oxygen from a sulfate anion in the solid $VOSO_4$. There is also a clear peak ascribed to the sulfate anion in Fig. 4a between 2.2 Å and 2.8 Å. Our analysis of the EXAFS results for the solid sample is consistent with literature reports [45,71,75,79]. The coordination number of water derived from the solid $VOSO_4$ were used to determine the ΔE_0 and S_0^2 parameters, essential for

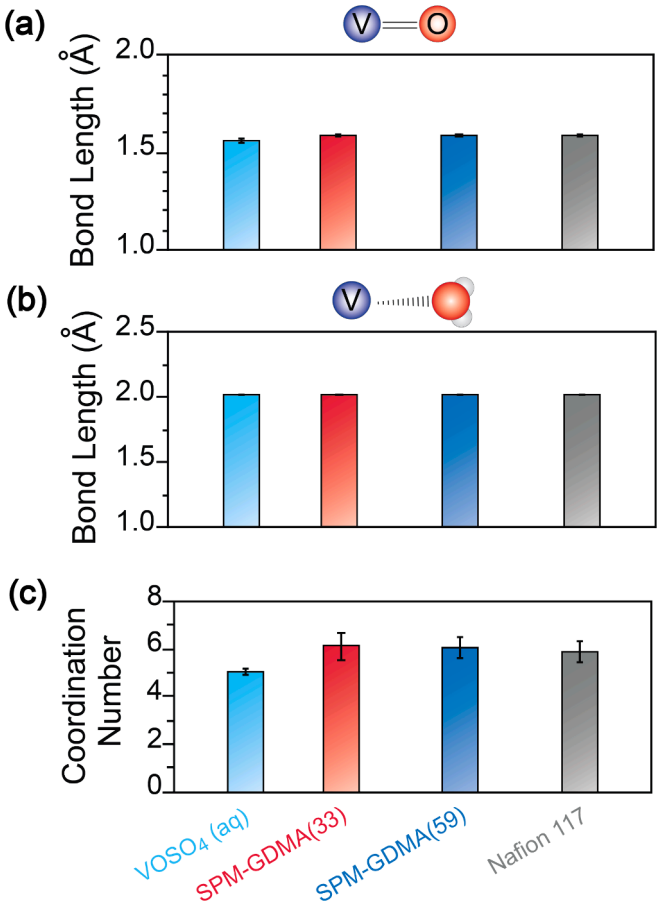

Fig. 5. Fitted parameters for VO^{2+} in an aqueous $VOSO_4$ solution and in the SPM-GDMA(33), SPM-GDMA(59), and Nafion 117 membranes. (a) Bond lengths for the double bonded oxygen in the vanadyl ion obtained from EXAFS fitting. (b) Bond lengths for the single bonded oxygen between vanadium and water ligands obtained from EXAFS fitting. (c) Coordination number of single bonded oxygen molecules around the vanadium ion. Bond length and coordination numbers are derived from EXAFS fitting of the data presented in Fig. 4. See Table S5 for details on all obtained fit parameters. Schematics above Fig. 5a and b show the bonds modelled by the EXAFS fitting.

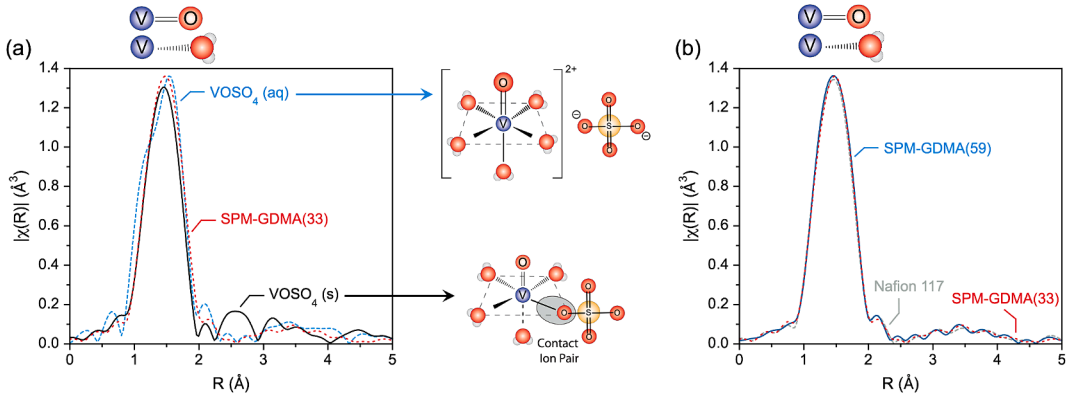

Fig. 4. a) k^2 weighted V K-edge EXAFS results for solid $VOSO_4$, aqueous $VOSO_4$, and VO^{2+} in SPM-GDMA(33). The peak between 1 to 2 Å is from electron backscattering due to the V=O bond and the coordination between the vanadyl cation and oxygen atoms in water. A schematic of these bonds is shown to the right of the blue arrow. The features between 2.2 and 2.8 Å are the primary difference between the solid sample and all other samples and are attributed to a sulfonate group oxygen forming a contact ion pair with vanadyl in the solid $VOSO_4$. The distance corresponds to electron backscattering of the V-O-S bond of the sulfate ion pair. The schematics in the middle illustrate the proposed structure of vanadyl in the solid (bottom) and aqueous (top) $VOSO_4$. (b) k^2 weighted EXAFS results for VO^{2+} in Nafion 117, SPM-GDMA(59), and SPM-GDMA(33) membranes. No evident differences were observed for the VO^{2+} in different membranes. (For interpretation of the references to colour in this figure legend, the reader is referred to the web version of this article.)

normalizing the fit and calculating the coordination number of oxygen atoms around the vanadyl ion in the aqueous and membrane samples. The fitting of the $VOSO_4$ (aq) EXAFS results reflected the expected structure shown in Fig. 4a. For $VOSO_4$ (aq), the double bonded oxygen group is present at a bond length of 1.58 Å, similar to the bond length in the solid $VOSO_4$, as shown in Fig. 5a. The aqueous $VOSO_4$ fit revealed that 5 oxygen atoms surround the vanadium ion at similar distances of just over 2 Å (Fig. 5b,c). To determine whether one of those oxygen atoms was coming from the sulfate anion, we attempted to include a sulfate anion into the fit (Table S5). However, inclusion of a sulfate anion was possible only if the V=O rattle path (where the electron scatters between the vanadium ion and the double-bonded oxygen atom twice) characteristic of the VO^{2+} ion, was absent. This scenario contradicts the known chemistry. Consequently, the sulfate anion is dissociated from the vanadyl cation in solution, suggesting that all five oxygen atoms in the first coordination shell of VO^{2+} in the aqueous solution of $VOSO_4$ are likely from water molecules.

The fitting results for all of the membranes were similar to those for the aqueous $VOSO_4$, as depicted in Fig. 5a and b. Each of the three membranes exhibited similar radial structure functions, bond lengths, and coordination numbers. The primary difference between the aqueous sample and the membrane samples is an extra coordination number of oxygen atoms in the membrane samples (Fig. 5c). While the assignment of this additional oxygen atom is uncertain, possible sources include an extra water molecule, the sulfonate group, or the carboxyl group on the polymer backbone. Further attempts to identify the source of the extra oxygen atom by including either the sulfonate or carboxyl groups during fitting resulted in unphysical values. Additionally, the higher uncertainty in the coordination number for the membrane samples suggests that the observed difference might be insignificant. Nevertheless, these results demonstrate that the coordination numbers of the vanadyl ions in the membrane are not lower than those in solution (Fig. 5c).

The results from XANES, UV–Vis, and EXAFS confirm that the local structure of vanadyl in aqueous solution and in the membranes is similar. Previous studies that have implemented XAFS with other transition metal cations in Nafion membranes and sulfonated cation exchange resins have reached similar conclusions [49–53,55]. For example, studies using EXAFS have demonstrated that Zn^{2+} and Ni^{2+} maintain their first water coordination shell when incorporated into Nafion membranes [50,51,53]. Similarly, the electronic state and coordination number of Sr^{2+} in the cation-exchange resin Amberlite 200CT equilibrated in DI water were found to be the same as those in aqueous solutions of $SrCl_2$ [55]. These observations suggest that cations do not dehydrate or form contact ion pairs with the sulfonate groups in these membranes even as the membrane water content decreases, provided there is enough water to satisfy the first hydration shells of the counter-ions and fixed charged groups [29]. Furthermore, across the various materials examined in these studies, neither the specific polymer matrix nor the sulfonate charged groups appeared to significantly alter the local environment of the counter-ions [53,54].

As previously mentioned, the coordination number refers to the average number of water molecules in direct contact with an ion, while the hydration number represents the average number of water molecules accompanying an ion during diffusion. Distinguishing between these two parameters is crucial for accurately interpreting experimental transport data and describing ion dehydration. We propose a method to relate coordination numbers obtained by EXAFS to hydration numbers via the residence time of water molecules in the first hydration shell of hydrated vanadyl (Section S6.4). Using data for the kinetics of water exchange reactions in the first hydration shell of vanadyl, we estimated that the residence time of the equatorial and axially coordinated waters around the first coordination shell of vanadyl is longer on average than the relaxation time of vanadyl diffusion and the residence time of water in pure water. The significant differences between these time scales and the similar bond distances between the equatorial and axially coordinated water molecules and the vanadyl ion (see Fig. 5b) suggest that both types of water molecules can be classified as hydration waters. This assumption has been recently explored via high flux backscattering (HFBS) quasi-elastic neutron scattering (QENS) measurements of vanadyl counter-ion diffusion in Nafion 117 [81]. In this study, the HFBS-QENS measurements captured the diffusion of water molecules involved in the hydration of the mobile vanadyl counter-ions, allowing for the study of the jump and local diffusion of vanadyl within Nafion 117 membranes. The study found that the smallest radius of the sphere at which the dynamics of the hydrated vanadium were observed (~5.42 Å) was larger than that of pure water (~3.66 Å). This finding suggests that the dynamics of vanadyl counter-ions in a water-equilibrated Nafion 117 membrane, measured via HFBS-QENS, originate from the hydrated ion [81].

The total water content of an IEM is pivotal when considering the potential for ion dehydration within the membrane. The membrane hydration number, λ, represents the number of water molecules in the membrane per fixed charge group/counter-ion pair. This number is instrumental in assessing whether sufficient water is present to maintain ion hydration levels comparable to those in aqueous solutions. If λ is smaller than the number of water molecules needed to fully hydrate the counter-ions and fixed charge groups as they are in solution, ion dehydration within the membrane is likely to occur due to insufficient availability of water molecules. This concept is empirically supported by Volkov et al., who used NMR to measure the hydration number of lithium ions in a Nafion membrane equilibrated with different relative humidities [82]. Their findings indicated that when $\lambda > 10$, the hydration number of lithium in Nafion is similar to that found in aqueous solutions. Conversely, at lower λ values, a notable chemical shift difference in the measured ^{7}Li NMR signal was observed, indicating ion dehydration [82].

The total amount of water in IEMs is generally categorized into freezable water and bound (i.e., non-freezable) water [11,83]. Freezable water includes bulk-like and weakly interacting water capable of undergoing thermal phase transitions such as freezing and melting. Conversely, bound water does not undergo a melting thermal phase transition at the same temperatures as freezable water presumably due to strong interactions between the water molecules and their environment (e.g., ions and polar groups on the polymer). These two states of water can be quantified via differential scanning calorimetry (DSC) as

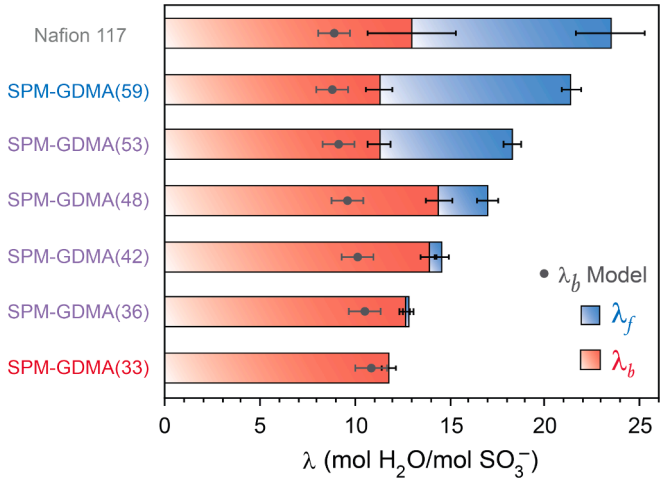

Fig. 6. The membrane hydration number, λ, decoupled into the bound water hydration number, λ_b, and freezable water hydration number, λ_f, for membranes in the VO^{2+} counter-ion form. The filled dark gray symbols represent the predicted values of λ_b by assuming all of the bound water resides in the primary coordination shell of the ions and hydroxyl group on the polymer. Uncertainties for the measured values represent the standard deviation of measurements performed on at least 8 independent samples. Uncertainties of the predicted values of λ_b were obtained via standard propagation of uncertainty techniques.

discussed in Section S7 [11,83–85]. Subsequently, the membrane hydration number λ can be decoupled into a freezable water hydration number, λ_f, and bound water hydration number, λ_b. As depicted in Fig. 6, SPM-GDMA(59) and Nafion 117 have approximately equal amount of freezable water and bound water, while virtually all of the water in the low water content membrane SPM-GDMA(33) is bound.

We modeled the bound water hydration number by accounting for contributions from the primary coordination shells of the vanadyl counter-ions, fixed charge groups, and water molecules interacting strongly with hydrophilic parts of the polymer (e.g., –OH groups in the case of SPM-GDMA membranes). These values of λ_b were estimated based on numerical assignments to these components, with the hydration of vanadyl ions equated to the first-shell water coordination numbers obtained from the EXAFS analysis (see Section S6.3 and Table S5). As shown in Fig. 6, the λ_b values predicted by the model are lower than the λ_b measured experimentally. The additional bound water may be from water interacting with the polymer or second-shell coordinated water. The total membrane hydration number, λ, being larger than the expected bound water hydration number, λ_b, indicates that the membranes contain a sufficient amount of water to fully hydrate the vanadyl ions and fixed charge groups. Collectively, the results from DSC and EXAFS analysis provide complementary evidence to support the conclusion that vanadyl ion dehydration does not occur, at least from the first hydration shell of the ions, in the membranes studied. Given that all of the water in SPM-GDMA(33) is bound, ion dehydration is likely to occur if the total water content of the membrane were reduced. However, synthesizing membranes with even lower water content than that of SPM-GDMA(33) was not possible. This difficulty arose because the mixture of SPM (solid powder) and GDMA (viscous liquid) required water to form a homogeneous solution. Attempts to use less water than in SPM-GDMA(33) led to the pre-polymer solution precipitating at room temperature. Consequently, reducing the water content further was not pursued.

It is important to address the limitations of the results discussed thus far in the EXAFS analysis. Due to the noise in our results at distances greater than 3.5 Å, fitting the second coordination shell proved challenging. This inability to accurately characterize the second coordination shell means that some aspects of the local environment of the ion and its solvation dynamics remain unexplored. It is possible that as vanadyl ions transition from the solution into the membrane, they lose second coordination shell water molecules. Techniques such as quasi-elastic neutron scattering [86], terahertz spectroscopy [87], and dielectric relaxation spectroscopy [88] could be employed to uncover more direct information about changes in the second coordination shells of vanadyl ions as they transition from the solution into the membrane. The larger measured values of λ_b compared to the predicted values in Fig. 6 could be attributed to additional bound waters associated with secondary coordination shells of vanadyl. The residence time of water in the second coordination shell of vanadyl has been hypothesized to be longer than 10^{-10} s [89], which would also qualify the expected eight water molecules on the phases of the vanadyl octahedral complex as hydration shell waters (*cf.* $\sim 10^{-11}$ s for pure water) [68,89].

Extending the XAFS results to other ions in membranes may be challenging. Vanadyl ions hold their water molecules more tightly than common alkali ions, as indicated by water exchange reaction rate measurements on the first hydration shell of the ions [89,90]. Thus, our method for correlating hydration and coordination numbers may not apply to alkali ions. Additionally, for some ions, obtaining reliable XAFS results is challenging due to their intrinsic attenuation length. If the attenuation length is significantly shorter or longer than the membrane thickness, it is challenging to obtain sufficient signal to noise ratio for accurate fitting. See Table S6 and S7 for more details regarding XAFS studies for various ions in membranes. With adjustments to membrane thickness, use of fluorescence detection, or with high flux x-ray sources the structure of these ions in membranes could also be determined.

2.4. Diffusion of vanadyl within the membranes

The mechanism of ion transport in IEMs involves ion partitioning into the membrane followed by diffusion down an electrochemical potential gradient. In this study, we investigated VO^{2+} diffusion in the CEMs and assessed the impact of membrane water content. Several factors could influence counter-ion diffusion as the membrane water content decreases, including the chemical structures of the fixed charge group and polymer [91], polymer dynamics [92–95], interactions between counter-ions and fixed charges [61,64,96–98], ion dehydration [14], and ion pairing [99–103]. Our preceding analyses indicate that the VO^{2+} counter-ions in the membranes maintain their first hydration shell and there are no detectable contact ion pairs between the fixed charge groups and VO^{2+}. Thus, the potential impact of ion dehydration and contact ion pairing on vanadyl counter-ion diffusion in these CEMs can be considered minimal.

We determined the VO^{2+} diffusion coefficients, D_V^m, from ionic conductivity measurements on membranes equilibrated with DI water via the Nernst-Einstein equation [12].

$$D_V^m = \frac{RT}{F^2}\frac{\kappa}{z_V^2 C_V^m} \tag{1}$$

where R is the gas constant, F is Faraday's constant, T is absolute temperature, κ is the membrane ionic conductivity, z_V is the VO^{2+} valence, and C_V^m is the VO^{2+} concentration in the membrane (in units of mol/L [membrane]). Measuring the ionic conductivity of DI water-equilibrated membranes ensures that the electrical current is carried solely by the vanadyl VO^{2+} counter-ions, thus avoiding interferences from other ions when the membrane contacts a salt solution. Eq. (1) assumes the validity of the Einstein equation, which relates ion mobility to ion diffusivity [12]. This assumption is reasonable for IEMs, particularly in the absence of co-ions, which can interact with the counter-ions and invalidate the Einstein equation [104].

Fig. 7 presents the ratio of the VO^{2+} diffusion coefficient in the

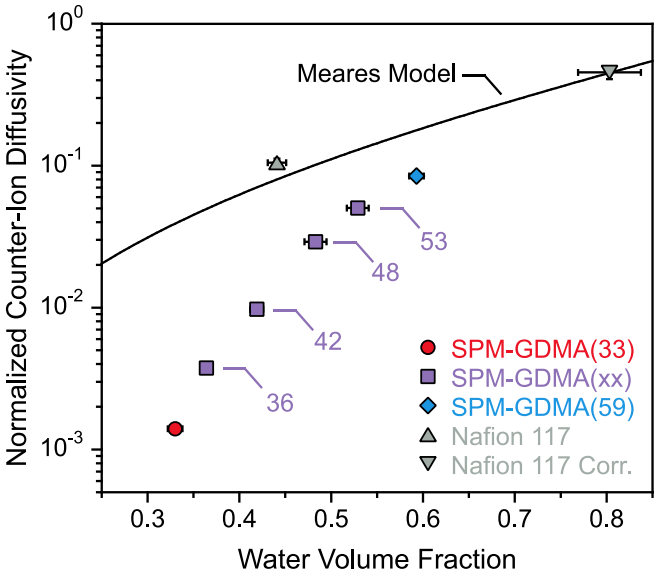

Fig. 7. Ratio of vanadyl counter-ion diffusion coefficient in the membrane, D_V^m, to that in an aqueous solution at infinite dilution, D_V^s. The solid line represents the prediction from the Meares model. The xx in SPM-GDMA(xx) represents the water volume percent in the membranes as indicated by the numbers next to the symbols. Uncertainties were determined via standard propagation of uncertainty techniques using results from measurements on at least ten samples. Results for Nafion are plotted both using the overall water volume fraction (Nafion 117) and using the water volume fraction of only the hydrophilic phase of Nafion (Nafion 117 Corr.).

membrane to that in an aqueous solution at infinite dilution, D_V^s, plotted against the water volume fraction of each membrane. For Nafion 117, two scenarios are depicted—one assumes a homogeneous membrane and uses the overall water volume fraction, while the other assumes a phase separated membrane and uses the water volume fraction of the hydrophilic phase (see Section S4.2). Additionally, Fig. 7 also includes diffusion coefficients predicted by the Meares tortuosity model, a widely implemented model in the study of ion diffusion in swollen polymers [105]. This simple model assumes that ion diffusion in the membrane follows a mechanism similar to that in an aqueous solution, but the relatively immobile polymer chains lengthen the diffusional path of the ions compared to an aqueous solution of equivalent thickness [105,106]. As a result, a higher polymer content (i.e., lower water volume fraction) creates a more tortuous pathway, which reduces ion diffusion coefficients. This model neglects specific interactions between the polymer and ions. The key result of this model is:

$$\frac{D_V^m}{D_V^s} = \left(\frac{\phi_w}{2-\phi_w}\right)^2 \tag{2}$$

where ϕ_w is the water volume fraction of the membrane.

For Nafion 117, assuming a homogeneous membrane structure in the diffusion analysis results in significantly higher normalized VO^{2+} diffusion coefficient compared to the homogeneous SPM-GDMA membranes. This discrepancy is not surprising given that Nafion is well known to phase separate into hydrophilic and hydrophobic domains [62]. When the effect of phase separation is considered in the analysis by assuming ion diffusion occurs primarily in the hydrophilic phase, the results for Nafion follow a similar trend as those for the SPM-GDMA membranes. For the SPM-GDMA membranes, the Meares model overestimates the VO^{2+} diffusion coefficients for all of the membranes. The discrepancy between model prediction and experiment becomes more pronounced as the membrane water content decreases. The largest discrepancy—approximately an order of magnitude—is observed for the lowest water content membrane. These findings suggest that factors beyond tortuosity, such as specific ion-polymer interactions or changes in the local environment of the ions, significantly influence VO^{2+} diffusion in membranes with reduced water content.

2.5. Activation energy and entropy of diffusion for vanadyl within the membranes

To develop better mechanistic understanding of VO^{2+} diffusion in the CEMs, we determined the diffusion coefficients across a temperature range of 10–60 °C and interpreted the results within the framework of transition state theory [11,107]. This approach, which views ion diffusion in the membrane as an activated process, has recently regained popularity for describing ion diffusion in polymer membranes [107]. According to the Eyring-Polanyi equation, the diffusion coefficient of VO^{2+} in the membrane is given by [11,97,107].

$$D_V^m = l^2\frac{k_B T}{h}\exp\left[\frac{\Delta S^{\ddagger}}{R}+1\right]\exp\left[-\frac{E_a^m}{RT}\right] \tag{3}$$

where l is the mean distance of a diffusion step, k_B is the Boltzmann constant, h is the Planck constant, E_a^m is the activation energy of diffusion, $\Delta S^{\ddagger}$ is the activation entropy of diffusion, and the other variables have been defined previously. The activation entropy of diffusion, indicative of the number of microstates an ion can occupy in the transition state relative to the equilibrium state, helps explain steric effects influencing ion diffusion [11,107]. Conversely, the activation energy of diffusion, representing the energy barrier ions must overcome during diffusion, primarily reflects the interactions between the ion and its local environment [11,107].

Fig. 8 presents the E_a^m and $\Delta S^{\ddagger}$ values for VO^{2+} across all of the membranes, plotted against their water volume fraction. For comparison, the activation energy (E_a^s) and activation entropy ($\Delta S^{\ddagger,s}$) of diffusion for VO^{2+} in an aqueous solution at infinite dilution are also shown to evaluate the impact of the membrane on VO^{2+} transport. In the case of Nafion 117 and SPM-GDMA(59), which are membranes with relatively high water content, the activation energy of diffusion in the membrane is approximately 17 % and 24 % higher, respectively, than in an aqueous solution. This result indicates that ion diffusion in these high water content membranes is not substantially different from that in an aqueous solution, likely because interactions between vanadyl and the fixed charges on the polymer are adequately screened by the abundant freezable water in the membranes. Conversely, for the lower water content SPM-GDMA membranes, E_a^m increases significantly as the water volume fraction of the membranes decreases. Notably, for the lowest

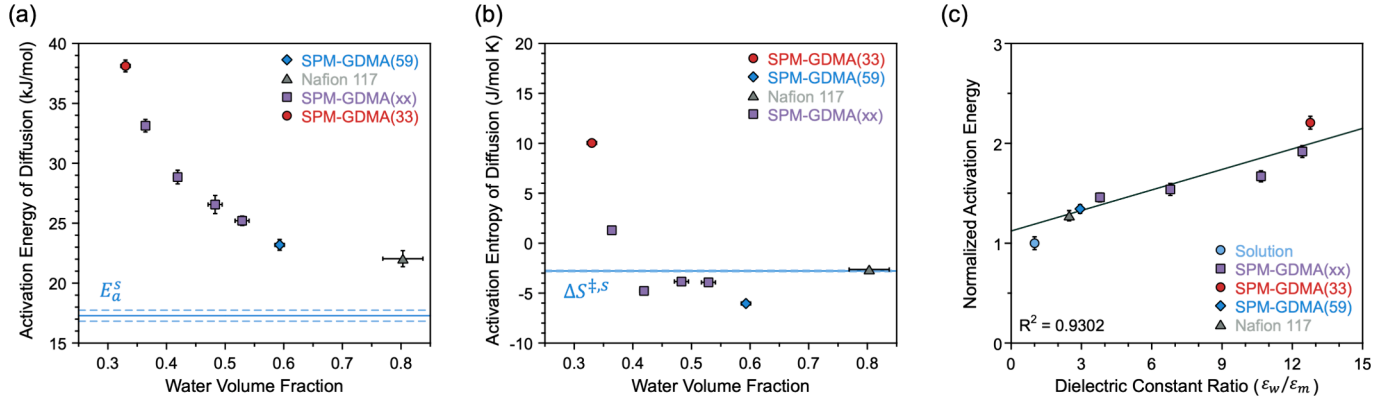

Fig. 8. (a) Activation energy of vanadyl diffusion in membranes of different water volume fractions. The solid blue line represents the solution activation energy of diffusion at infinite dilution (E_a^s), and the dashed lines represent the uncertainty of this parameter determined from the fitting procedure (Section S8.7). (b) Activation entropy of vanadyl diffusion in the membranes as a function of water volume fraction. The solid blue line represents the solution activation entropy of diffusion at infinite dilution ($\Delta S^{\ddagger,s}$) and the dashed lines represent the uncertainty of this parameter determined from the fitting procedure (Section S8.7). The activation entropy associated with the diffusion process was calculated from the pre-exponential factor obtained from the linearized Arrhenius equation and the Eyring-Polanyi equation relating entropy to the pre-exponential factor (Eq. (3)) assuming a jump distance of 2.8 Å (i.e., the size of a water molecule) [11,108] for both the solution and the membrane. Uncertainties of the measured E_a^m and $\Delta S^{\ddagger}$ were determined via standard propagation of uncertainty techniques using results from measurements on at least three membrane samples. (c) The normalized activation energy of diffusion (E_a^m/E_a^s) plotted against $\varepsilon_w/\varepsilon_m$, where ε_w and ε_m are the dielectric constants of pure water and the membrane, respectively. A linear trend line is included to fit the data with the R^2 value indicated. (For interpretation of the references to colour in this figure legend, the reader is referred to the web version of this article.)

water content membrane, the activation energy of diffusion is nearly double that in the aqueous solution, suggesting a significant influence of the membrane on VO^{2+} diffusion.

A recent study has linked variations in the activation energies of diffusion/permeation to ion dehydration within the membrane [14]. The study reported that ions with smaller ionic radii and higher hydration energies exhibit higher activation energies of permeation in IEMs, attributing this to ion dehydration at the membrane/solution interface. Similar conclusions have been reached in studies exploring the activation energy of transport in nanofiltration membranes and molecular dynamics simulations of nanopores formed by graphene and carbon nanotubes [23,109]. In the case of VO^{2+} ions in the membranes studied here, dehydration of the first hydration shell does not occur, making this explanation insufficient to account for the changes in the activation energies of diffusion. In a previous study, we observed similar behavior for various monovalent cations (Li^+, Na^+, K^+, and Cs^+) in the same SPM-GDMA membranes studied here, where the activation energies of diffusion significantly increased with decreasing membrane water content [11]. We attributed this result to stronger Coulombic interactions between the fixed charge groups and counter-ions, which become more pronounced as the dielectric constant of the membrane decreases with decreasing water content. The increase in activation energy of diffusion was adequately predicted without adjustable parameters by a model incorporating Coulomb's law to calculate electrostatic interactions between the fixed charge groups and counter-ions [11].

In this model, we assumed that the energy barrier arises due to differences in Coulombic interactions between the fixed charge groups and counter-ions. Using Coulomb's law, we calculated the change in electrostatic energy between a counter-ion and a fixed charge group from an initial state to a final state after the counter-ion makes a diffusional jump. The distance between the ions in the initial state was approximated by considering the counter-ions and fixed charged groups are separated only by their hydration shell. The distance between the ions in the final state was approximated as the distance of the initial state plus the diameter of a water molecule (2.8 Å), which is consistent with diffusional jumps of ions in aqueous environments. The dielectric constant of the membrane was calculated as a volume fraction-weighted average dielectric constant containing the contribution from the polymer, the freezable water, and the bound water. The activation energy of diffusion in the membrane is composed of two parts: the intrinsic activation energy of diffusion in water (which accounts for the displacement of water molecules during diffusion) and the additional energy difference due to electrostatic interactions between the fixed charges and the counter-ions [11].

The model only considered the diffusional jump of a monovalent counter-ion away from a single fixed charge group, and efforts are under way to extend its application for divalent counter-ions ions like vanadyl. Nevertheless, we hypothesize that similar physical phenomena account for the observed results for VO^{2+}. To demonstrate the importance of Coulombic interactions in influencing VO^{2+} diffusion in the CEMs, Fig. 8c shows the normalized activation energy of diffusion in the membrane plotted against the ratio of the dielectric constant of bulk water to that of the membrane. The membrane dielectric constant was estimated as a volume fraction weighted average of the dielectric constants of the polymer, freezable water, and bound water as previously reported [11]. A strong correlation is observed between the normalized activation energy of diffusion and dielectric constant ratio. That is, as the membrane dielectric constant decreases due to a smaller fraction of freezable water, the normalized activation energy of diffusion increases due to stronger Coulombic interactions between the fixed charge groups and counter-ions. This linear correlation is anticipated since the interaction energy from Coulombic interactions scales inversely with the dielectric constant of the medium (i.e., the membrane dielectric constant, ε_m).

The activation entropy of diffusion, $\Delta S^{\ddagger}$, which represents the change in entropy between the activated state and the equilibrium state, provides additional insights into the mechanism of ion diffusion in polymers. In previous studies of ion diffusion, positive $\Delta S^{\ddagger}$ values have been attributed to the breakage of bonds or structural changes during the activation process [97]. Conversely, negative $\Delta S^{\ddagger}$ values have been attributed to electrostriction of water around the ions in the activated state [110], which reduces the molecular degrees of freedom. As shown in Fig. 8b, the activation entropies for all membranes, except for SPM-GDMA(33) and SPM-GDMA(36) which have the lowest water content, are comparable in magnitude. Furthermore, these values are negative, indicating that the molecular degrees of freedom in the activated state are fewer than in the equilibrium state. This result is reasonable, considering that divalent cations must be electrically balanced by two fixed charge groups on the polymer backbone. As an ion executes a diffusion step away from the fixed charge groups, there are fewer possible microstates than when the ion is at equilibrium. This view contrasts with the situation in an aqueous solution, where the counter-anions (e.g., sulfate) to VO^{2+} are also mobile.

For SPM-GDMA(33), the activation entropy of diffusion is positive and larger than that of the aqueous solution. This increase in activation entropy relative to the higher water content membranes can result from increasing the entropy of the activated state, decreasing the entropy of the equilibrium state, or both. The DSC results indicate that virtually all the water molecules in SPM-GDMA(33) are bound, reducing the fraction of accessible microstates and thus lowering the entropy of the equilibrium state. Additionally, the increased Coulombic interactions between the counter-ions and fixed charges in SPM-GDMA(33), as evidenced by the higher activation energy, could further reduce the entropy of the equilibrium state by limiting the molecular degrees of freedom of the divalent ions between two charged groups. Executing a diffusion step in SPM-GDMA(33) will require the temporary breaking and rearrangement of the bound water structure in the membranes, which will increase the number of accessible microstates in the transition state. Thus, the entropy of the activated state is higher than the entropy of the equilibrium state due to the necessity of a temporarily broken or rearranged structure of hydration water upon making a diffusional jump. This result agrees with previous results for monovalent ions in these SPM-GDMA membranes, where the activation entropies of diffusion increased substantially at low membrane water content [11].

3. Conclusions

In this study, we investigated the local molecular environment of vanadyl cations in a series of negatively charged polymer membranes with broadly varying water volume fractions (from 0.33 to 0.59) using x-ray absorption fine structure spectroscopy (XAFS). The results indicate that the oxidation state and the electronic structure of vanadyl counter-ions were similar to those in an aqueous solution of vanadyl sulfate. Additionally, the primary coordination shell of the vanadyl counter-ion in the membranes was similar to that found in solution of vanadyl sulfate, with approximately five water molecules in the first coordination shell. This suggests that the vanadyl cations do not dehydrate or form contact ion pairs within the membranes. These findings were rationalized by considering the strength of interactions between vanadyl cations and the water molecules in the primary coordination shell, as quantified by the reaction rate for water exchange between the primary coordination shell and the bulk solution, and the availability of water within the membranes, as quantified by differential scanning calorimetry. The conclusions derived from this study are likely to apply to other cations that exhibit similar reaction rates (smaller than 10^8 s^{-1}) for water exchange between the primary coordination shell and the bulk solution. Notably, cations of interest for desalination applications, such as alkali cations, exhibit substantially higher water exchange reaction rates than vanadyl, posing a limitation in the generality of our findings. Future work on the XAFS studies on these cations within charged membranes would reveal whether they dehydrate upon partitioning in the

membrane.

We also measured the diffusion coefficients of the vanadyl cations in the membranes, as well as their activation energy and entropy of diffusion. The diffusion coefficients decrease by two orders of magnitude while the activation energy of diffusion increases by approximately a factor of two from the highest to the lowest water content membranes studied in this work. These differences were attributed to stronger Coulombic interactions between the vanadyl cations and fixed charged groups within the membrane, rather than the commonly invoked explanation of ion dehydration within the membrane. As the freezable water content of the membranes decreases from 11 to almost 0, the dielectric constant of the membranes also decreases from approximately 25–5.5, strengthening the Coulombic interactions between the vanadyl cations and fixed charge groups.

For all membranes excluding SPM-GDMA(33), the activation entropy is negative, indicating that the entropy in the equilibrium state is greater than in the activated state, as the structure of the activated ion is more restricted. This behavior likely results from two charged groups neutralizing the counter-ion, which reduces the microstates available for the ion within the polymer. However, in SPM-GDMA(33), the activation entropy is positive, likely due to both a decrease in the entropy of the equilibrium state and an increase in the entropy of the activated state. The DSC results indicate that this membrane has no freezable water molecules, so a vanadium ion within the membrane has significantly fewer degrees of freedom, leading to a lower entropy in the equilibrium state. Conversely, taking a diffusional jump in the low water content environment of the SPM-GDMA(33) membrane could require rearrangement of the hydration layers, including breaking of bonds with the bound waters of hydration, resulting in an increase in entropy in the activated state.

Associated content

Additional experimental details and results (states of water, ionic conductivity, activation energy of diffusion, small angle x-ray scattering, X-ray absorption fine structure) are included in the Supplementary information. All of the numerical data are tabulated in the Supplementary Data sheet.

CRediT authorship contribution statement

José C. Díaz: Writing – review & editing, Writing – original draft, Validation, Investigation, Formal analysis, Data curation. **Christina E. Uhlenbrock:** Writing – review & editing, Writing – original draft, Validation, Investigation, Formal analysis, Data curation. **Nirala Singh:** Writing – review & editing, Supervision, Project administration, Funding acquisition, Formal analysis. **Jovan Kamcev:** Writing – review & editing, Supervision, Project administration, Funding acquisition, Formal analysis, Conceptualization.

Declaration of competing interest

The authors declare the following financial interests/personal relationships which may be considered as potential competing interests: Jovan Kamcev and José C. Díaz have patent #PCT/US22/18826 pending to University of Michigan. If there are other authors, they declare that they have no known competing financial interests or personal relationships that could have appeared to influence the work reported in this paper.

Data availability

The data presented in this manuscript is included in the Supplementary information.

Acknowledgements

This material is based upon work supported by the U.S. Department of Energy, Office of Science, Basic Energy Sciences under Award Number DE-SC0022040. N.S. acknowledges funding from NSF Grant # 2236770. J.C.D. would like to acknowledge support from the National Defense Science and Engineering Graduate (NDSEG) Fellowship Award supported by the Office of Naval Research (ONR). The authors acknowledge the use of facilities supported by the Laboratory for Research on the Structure of Matter and the NSF through the University of Pennsylvania Materials Research Science and Engineering Center (MRSEC) DMR-2309043. We thank Dr. Iryna Golovina form MRSEC for help in collecting the SAXS spectra of the vanadyl-form membranes. This research used resources of the Advanced Photon Source, a U.S. Department of Energy (DOE) Office of Science user facility operated for the DOE Office of Science by Argonne National Laboratory under Contract No. DE-AC02-06CH11357. XAFS data was collected at beamline 20-BM. Sector 20 operations are supported by the US Department of Energy and the Canadian Light Source. We thank Dr. Chengjun Sun and Dr. Harsh Agarwal for their help in collecting V K-edge spectra. We thank David Kitto for fruitful discussions on accurately fitting the linearized Arrhenius equation using the general least-squares fitting method. We thank Rahul Sujanani for fruitful discussion on accounting for the phase separated morphology of Nafion 117 when considering ion transport across this membrane.

Appendix A. Supplementary data

Supplementary data to this article can be found online at https://doi.org/10.1016/j.cej.2024.155942.

References

[1] T. Luo, S. Abdu, M. Wessling, Selectivity of ion exchange membranes: a review, J. Membr. Sci. 555 (2018) 429–454, https://doi.org/10.1016/j.memsci.2018.03.051.
[2] R.M. DuChanois, C.J. Porter, C. Violet, R. Verduzco, M. Elimelech, Membrane materials for selective ion separations at the water-energy nexus, Adv. Mater. 33 (2021) 2101312, https://doi.org/10.1002/adma.202101312.
[3] Strathmann, Heiner, Ion-Exchange Membrane Separation Processes, Elsevier, 2004.
[4] H. Fan, Y. Huang, N.Y. Yip, Advancing ion-exchange membranes to ion-selective membranes: principles, status, and opportunities, Front. Environ. Sci. Eng. 17 (2022) 25, https://doi.org/10.1007/s11783-023-1625-0.
[5] D. Kitto, J. Kamcev, Predicting the conductivity–selectivity trade-off and upper bound in ion-exchange membranes, ACS Energy Lett. (2024) 1346–1352. https://doi.org/10.1021/acsenergylett.4c00301.
[6] R.M. DuChanois, N.J. Cooper, B. Lee, S.K. Patel, L. Mazurowski, T.E. Graedel, M. Elimelech, Prospects of metal recovery from wastewater and brine, Nat. Water 1 (2023) 37–46, https://doi.org/10.1038/s44221-022-00006-z.
[7] X. Shi, O.C. Esan, X. Huo, Y. Ma, Z. Pan, L. An, T.S. Zhao, Polymer electrolyte membranes for vanadium redox flow batteries: fundamentals and applications, Prog. Energy Combust. Sci. 85 (2021) 100926, https://doi.org/10.1016/j.pecs.2021.100926.
[8] C.H.L. Tempelman, J.F. Jacobs, R.M. Balzer, V. Degirmenci, Membranes for all vanadium redox flow batteries, J. Storage Mater. 32 (2020) 101754, https://doi.org/10.1016/j.est.2020.101754.
[9] B. Schwenzer, J. Zhang, S. Kim, L. Li, J. Liu, Z. Yang, Membrane development for vanadium redox flow batteries, ChemSusChem 4 (2011) 1388–1406, https://doi.org/10.1002/cssc.201100068.
[10] R. Wang, S. Lin, Membrane design principles for ion-selective electrodialysis: an analysis for Li/Mg separation, Environ. Sci. Tech. 58 (2024) 3552–3563, https://doi.org/10.1021/acs.est.3c08956.
[11] J.C. Díaz, J. Park, A. Shapiro, H. Patel, L. Santiago-Pagán, D. Kitto, J. Kamcev, Understanding monovalent cation diffusion in negatively charged membranes and the role of membrane water content, Macromolecules 57 (2024) 2468–2481, https://doi.org/10.1021/acs.macromol.3c02655.
[12] F.G. Helfferich, Ion Exchange, Dover ed., Dover Publications, New York, 1995.
[13] J. Kamcev, Reformulating the permselectivity-conductivity tradeoff relation in ion-exchange membranes, J. Polym. Sci. 59 (2021) 2510–2520, https://doi.org/10.1002/pol.20210304.
[14] R. Epsztein, E. Shaulsky, M. Qin, M. Elimelech, Activation behavior for ion permeation in ion-exchange membranes: role of ion dehydration in selective transport, J. Membr. Sci. 580 (2019) 316–326, https://doi.org/10.1016/j.memsci.2019.02.009.

[15] R. Epsztein, R.M. DuChanois, C.L. Ritt, A. Noy, M. Elimelech, Towards single-species selectivity of membranes with subnanometre pores, Nat. Nanotechnol. 15 (2020) 426–436, https://doi.org/10.1038/s41565-020-0713-6.

[16] C. Lu, C. Hu, C.L. Ritt, X. Hua, J. Sun, H. Xia, Y. Liu, D.-W. Li, B. Ma, M. Elimelech, J. Qu, In situ characterization of dehydration during ion transport in polymeric nanochannels, J. Am. Chem. Soc. 143 (2021) 14242–14252, https://doi.org/10.1021/jacs.1c05765.

[17] S.B. Sigurdardottir, R.M. DuChanois, R. Epsztein, M. Pinelo, M. Elimelech, Energy barriers to anion transport in polyelectrolyte multilayer nanofiltration membranes: role of intra-pore diffusion, J. Membr. Sci. 603 (2020) 117921, https://doi.org/10.1016/j.memsci.2020.117921.

[18] B. Tansel, J. Sager, T. Rector, J. Garland, R.F. Strayer, L. Levine, M. Roberts, M. Hummerick, J. Bauer, Significance of hydrated radius and hydration shells on ionic permeability during nanofiltration in dead end and cross flow modes, Sep. Purif. Technol. 51 (2006) 40–47, https://doi.org/10.1016/j.seppur.2005.12.020.

[19] X. Zhou, Z. Wang, R. Epsztein, C. Zhan, W. Li, J.D. Fortner, T.A. Pham, J.-H. Kim, M. Elimelech, Intrapore energy barriers govern ion transport and selectivity of desalination membranes, Sci. Adv. 6 (2020) eabd9045. https://doi.org/10.1126/sciadv.abd9045.

[20] I. Shefer, O. Peer-Haim, O. Leifman, R. Epsztein, Enthalpic and entropic selectivity of water and small ions in polyamide membranes, Environ. Sci. Tech. 55 (2021) 14863–14875, https://doi.org/10.1021/acs.est.1c04956.

[21] V. Pavluchkov, I. Shefer, O. Peer-Haim, J. Blotevogel, R. Epsztein, Indications of ion dehydration in diffusion-only and pressure-driven nanofiltration, J. Membr. Sci. 648 (2022) 120358, https://doi.org/10.1016/j.memsci.2022.120358.

[22] I. Shefer, O. Peer-Haim, R. Epsztein, Limited ion-ion selectivity of salt-rejecting membranes due to enthalpy-entropy compensation, Desalination 541 (2022) 116041, https://doi.org/10.1016/j.desal.2022.116041.

[23] L.A. Richards, B.S. Richards, B. Corry, A.I. Schäfer, Experimental energy barriers to anions transporting through nanofiltration membranes, Environ. Sci. Tech. 47 (2013) 1968–1976, https://doi.org/10.1021/es303925r.

[24] L.A. Richards, A.I. Schäfer, B.S. Richards, B. Corry, Quantifying barriers to monovalent anion transport in narrow non-polar pores, PCCP 14 (2012) 11633–11638, https://doi.org/10.1039/C2CP41641G.

[25] L.A. Richards, A.I. Schäfer, B.S. Richards, B. Corry, The importance of dehydration in determining ion transport in narrow pores, Small 8 (2012) 1701–1709, https://doi.org/10.1002/smll.201102056.

[26] H. Malmir, R. Epsztein, M. Elimelech, A. Haji-Akbari, Induced charge anisotropy: a hidden variable affecting ion transport through membranes, Matter 2 (2020) 735–750, https://doi.org/10.1016/j.matt.2019.12.022.

[27] M. Kanduč, W.K. Kim, R. Roa, J. Dzubiella, Aqueous nanoclusters govern ion partitioning in dense polymer membranes, ACS Nano 13 (2019) 11224–11234, https://doi.org/10.1021/acsnano.9b04279.

[28] Y. Marcus, G. Hefter, Ion pairing, Chem. Rev. 106 (2006) 4585–4621, https://doi.org/10.1021/cr040087x.

[29] R.A. Komoroski, K.A. Mauritz, A sodium-23 nuclear magnetic resonance study of ionic mobility and contact ion pairing in a perfluorosulfonate ionomer, J. Am. Chem. Soc. 100 (1978) 7487–7489, https://doi.org/10.1021/ja00492a008.

[30] R.A. Komoroski, K.A. Mauritz, Nuclear magnetic resonance studies and the theory of ion pairing in perfluorosulfonate ionomers, in: Perfluorinated Ionomer Membranes, American Chemical Society, 1982, pp. 113–138. https://doi.org/10.1021/bk-1982-0180.ch007.

[31] N.F.A. van der Vegt, K. Haldrup, S. Roke, J. Zheng, M. Lund, H.J. Bakker, Water-mediated ion pairing: occurrence and relevance, Chem. Rev. 116 (2016) 7626–7641, https://doi.org/10.1021/acs.chemrev.5b00742.

[32] B. Yu, B.M. Pettitt, J. Iwahara, Experimental evidence of solvent-separated ion pairs as metastable states in electrostatic interactions of biological macromolecules, J. Phys. Chem. Lett. 10 (2019) 7937–7941, https://doi.org/10.1021/acs.jpclett.9b03084.

[33] H. Liao, W. Zhong, C. Li, J. Han, X. Sun, X. Xia, T. Li, A. Noori, M.F. Mousavi, X. Liu, Y. Zhang, An intrinsically self-healing and anti-freezing molecular chains induced polyacrylamide-based hydrogel electrolytes for zinc manganese dioxide batteries, J. Energy Chem. 89 (2024) 565–578, https://doi.org/10.1016/j.jechem.2023.10.017.

[34] T. Han, C. Zhang, J. Luo, Macroscale superlubricity enabled by hydrated alkali metal ions, Langmuir 34 (2018) 11281–11291, https://doi.org/10.1021/acs.langmuir.8b01722.

[35] Q. Liu, Y. Luo, S. Yang, Y. Xiong, R. Wang, X. Fu, R. Zhang, S. Hu, X. Bao, C. Xu, Transfer-free *in-situ* synthesis of high-performance polybenzimidazole grafted graphene oxide-based proton exchange membrane for high-temperature proton exchange membrane fuel cells, J. Power Sources 559 (2023) 232666, https://doi.org/10.1016/j.jpowsour.2023.232666.

[36] V.-A. Glezakou, Y. Chen, J.L. Fulton, G.K. Schenter, L.X. Dang, Electronic structure, statistical mechanical simulations, and EXAFS spectroscopy of aqueous potassium, Theor. Chem. Acc. 115 (2006) 86–99, https://doi.org/10.1007/s00214-005-0054-4.

[37] L.X. Dang, G.K. Schenter, V.-A. Glezakou, J.L. Fulton, Molecular simulation analysis and X-ray absorption measurement of Ca2+, K+ and Cl- ions in solution, J. Phys. Chem. B 110 (2006) 23644–23654, https://doi.org/10.1021/jp064661f.

[38] J.L. Fulton, G.K. Schenter, M.D. Baer, C.J. Mundy, L.X. Dang, M. Balasubramanian, Probing the hydration structure of polarizable halides: a multiedge XAFS and molecular dynamics study of the iodide anion, J. Phys. Chem. B 114 (2010) 12926–12937, https://doi.org/10.1021/jp106378p.

[39] S. Ghosh, H. Agarwal, M. Galib, B. Tran, M. Balasubramanian, N. Singh, J. L. Fulton, N. Govind, Near-quantitative predictions of the first-shell coordination structure of hydrated first-row transition metal ions using K-edge X-ray absorption near-edge spectroscopy, J. Phys. Chem. Lett. 13 (2022) 6323–6330, https://doi.org/10.1021/acs.jpclett.2c01532.

[40] Y. Chen, J.L. Fulton, W. Partenheimer, A XANES and EXAFS study of hydration and ion pairing in ambient aqueous MnBr 2 solutions, J. Solution Chem. 34 (2005) 993–1007, https://doi.org/10.1007/s10953-005-6986-4.

[41] Y. Marcus, Ionic radii in aqueous solutions, Chem. Rev. 88 (1988) 1475–1498, https://doi.org/10.1021/cr00090a003.

[42] H. Ohtaki, T. Radnai, Structure and dynamics of hydrated ions, Chem. Rev. 93 (1993) 1157–1204, https://doi.org/10.1021/cr00019a014.

[43] A. Iglesias-Juez, G.L. Chiarello, G.S. Patience, M.O. Guerrero-Pérez, Experimental methods in chemical engineering: X-ray absorption spectroscopy—XAS, XANES, EXAFS, Can. J. Chem. Eng. 100 (2022) 3–22, https://doi.org/10.1002/cjce.24291.

[44] R.R. Pappalardo, D.Z. Caralampio, J.M. Martínez, E. Sánchez Marcos, Hydration of heavy alkaline-earth cations studied by molecular dynamics simulations and X-ray absorption spectroscopy, Inorg. Chem. 60 (2021) 13578–13587, https://doi.org/10.1021/acs.inorgchem.1c01888.

[45] J. Krakowiak, D. Lundberg, I. Persson, A coordination chemistry study of hydrated and solvated cationic vanadium ions in oxidation states +III, +IV, and +V in solution and solid state, Inorg. Chem. 51 (2012) 9598–9609, https://doi.org/10.1021/ic300202f.

[46] M. Harada, T. Okada, Local structures of ions at ion-exchange resin/solution interface, J. Chromatogr. A 1085 (2005) 3–7, https://doi.org/10.1016/j.chroma.2005.03.060.

[47] T. Aoki, M. Harada, T. Okada, Characterization of bromide ions in charge-stacked zwitterionic micellar systems, Langmuir 23 (2007) 8820–8826, https://doi.org/10.1021/la701145q.

[48] A. Yuchi, S. Kuroda, M. Takagi, Y. Watanabe, S. Nakao, Effects of the exchange capacity and cross-linking degree on the hydration states of anions in quantitative loading onto strongly basic anion-exchange resins, Anal. Chem. 82 (2010) 8611–8617, https://doi.org/10.1021/ac101707j.

[49] D.J. Yarusso, S.L. Cooper, G.S. Knapp, P. Georgopoulos, EXAFS analysis of cation environment in sulfonated polystyrene ionomers, J. Polym. Sci., Polym. Lett. Ed. 18 (1980) 557–562, https://doi.org/10.1002/pol.1980.130180808.

[50] H.K. Pan, D.J. Yarusso, G.S. Knapp, M. Pineri, A. Meagher, J.M.D. Coey, S. L. Cooper, EXAFS and Mössbauer studies of iron neutralized Nafion ionomers, J. Chem. Phys. 79 (1983) 4736–4745, https://doi.org/10.1063/1.445616.

[51] H.K. Pan, G.S. Knapp, S.L. Cooper, EXAFS and XANES studies of Zn2+ and Rb+ neutralized perfluorinated ionomers, Colloid Polymer. Sci. 262 (1984) 734–746, https://doi.org/10.1007/BF01451546.

[52] H.K. Pan, A. Meagher, M. Pineri, G.S. Knapp, S.L. Cooper, EXAFS studies of Fe3+ neutralized Nafion: interpretation of the second peak in the radial structure function, J. Chem. Phys. 82 (1985) 1529–1538, https://doi.org/10.1063/1.448428.

[53] H.K. Pan, D.J. Yarusso, G.S. Knapp, S.L. Cooper, EXAFS studies of nickel nafion ionomers, J. Polym. Sci. Polym. Phys. Ed. 21 (1983) 1389–1401, https://doi.org/10.1002/pol.1983.180210810.

[54] B.P. Grady, R.B. Moore, EXAFS studies of various sulfonated and carboxylated cadmium ionomers, Macromolecules 29 (1996) 1685–1690, https://doi.org/10.1021/ma951058e.

[55] M. Harada, T. Okada, Hydration of counterions in cation exchange resins studied by X-ray absorption fine structure, Chem. Commun. (2008) 5182–5184, https://doi.org/10.1039/B810997D.

[56] T. Okada, M. Harada, Hydration of halide anions in ion-exchange resin and their dissociation from cationic groups, Anal. Chem. 76 (2004) 4564–4571, https://doi.org/10.1021/ac049602h.

[57] M. Harada, T. Okada, I. Watanabe, Solvation structure of bromide ion in anion-exchange resins, J. Phys. Chem. B 106 (2002) 34–40, https://doi.org/10.1021/jp011390u.

[58] M. Harada, T. Okada, X-ray absorption fine structure of halide ions in anion-exchange resins, J. Ion Exch. 14 (2003) 25–28, https://doi.org/10.5182/jaie.14.Supplement_25.

[59] A.L. Maclean, G.J. Foran, B.J. Kennedy, EXAFS studies on Mn(III) tetraphenylporphyrin halides in Nafion, Inorg. Chim. Acta 268 (1998) 231–238, https://doi.org/10.1016/S0020-1693(97)05749-6.

[60] M. Vijayakumar, N. Govind, B. Li, X. Wei, Z. Nie, S. Thevuthasan, V. Sprenkle, W. Wang, Aqua-Vanadyl Ion Interaction with Nafion® Membranes, Front. Energy Res. 3 (2015), https://doi.org/10.3389/fenrg.2015.00010.

[61] H. Fan, Y. Huang, I.H. Billinge, S.M. Bannon, G.M. Geise, N.Y. Yip, Counterion mobility in ion-exchange membranes: spatial effect and valency-dependent electrostatic interaction, ACS EST Eng. 2 (2022) 1274–1286, https://doi.org/10.1021/acsestengg.1c00457.

[62] F.I. Allen, L.R. Comolli, A. Kusoglu, M.A. Modestino, A.M. Minor, A.Z. Weber, Morphology of hydrated As-cast nafion revealed through cryo electron tomography, ACS Macro Lett. 4 (2015) 1–5, https://doi.org/10.1021/mz500606h.

[63] A. Kusoglu, A.Z. Weber, New insights into perfluorinated sulfonic-acid ionomers, Chem. Rev. 117 (2017) 987–1104, https://doi.org/10.1021/acs.chemrev.6b00159.

[64] S. Shi, A.Z. Weber, A. Kusoglu, Structure-transport relationship of perfluorosulfonic-acid membranes in different cationic forms, Electrochim. Acta 220 (2016) 517–528, https://doi.org/10.1016/j.electacta.2016.10.096.

[65] H. Agarwal, J. Florian, B.R. Goldsmith, N. Singh, The Effect of anion bridging on heterogeneous charge transfer for V2+/V3+, Cell Rep. Phys. Sci. 2 (2021) 100307 https://doi.org/10.1016/j.xcrp.2020.100307.

[66] C. Lutz, S. Hampel, X. Ke, S. Beuermann, T. Turek, U. Kunz, A. Guilherme Buzanich, M. Radtke, U.E.A. Fittschen, Evidence for redox reactions during vanadium crossover inside the nanoscopic water-body of Nafion 117 using X-ray absorption near edge structure spectroscopy, J. Power Sources 483 (2021) 229176. https://doi.org/10.1016/j.jpowsour.2020.229176.

[67] T.R. Ortolano, J. Selbin, S.P. McGlynn, Electronic structure, spectra, and magnetic properties of oxycations. V. The electronic spectra of some vanadyl complexes, J. Chem. Phys. 41 (1964) 262–268. https://doi.org/10.1063/1.1725631.

[68] M. Vijayakumar, S.D. Burton, C. Huang, L. Li, Z. Yang, G.L. Graff, J. Liu, J. Hu, M. Skyllas-Kazacos, Nuclear magnetic resonance studies on vanadium(IV) electrolyte solutions for vanadium redox flow battery, J. Power Sources 195 (2010) 7709–7717, https://doi.org/10.1016/j.jpowsour.2010.05.008.

[69] M. Newville, B. Ravel, ATHENA, ARTEMIS, HEPHAESTUS: data analysis for X-ray absorption spectroscopy using IFEFFIT, J. Synchrotron. Rad. 12 (2005) 537–541, https://doi.org/10.1107/S0909049505012719.

[70] N.H. Choi, S. Kwon, H. Kim, Analysis of the oxidation of the V(II) by dissolved oxygen using UV-visible spectrophotometry in a vanadium redox flow battery, J. Electrochem. Soc. 160 (2013) A973, https://doi.org/10.1149/2.145306jes.

[71] J. Selbin, The chemistry of oxovanadium(IV), Chem. Rev. 65 (1965) 153–175, https://doi.org/10.1021/cr60234a001.

[72] J. Selbin, Oxovanadium(IV) complexes, Coord. Chem. Rev. 1 (1966) 293–314, https://doi.org/10.1016/S0010-8545(00)80142-3.

[73] C.V. Grant, W. Cope, J.A. Ball, G.G. Maresch, B.J. Gaffney, W. Fink, R.D. Britt, Electronic structure of the aqueous vanadyl ion probed by 9 and 94 GHz EPR and pulsed ENDOR spectroscopies and density functional theory calculations, J. Phys. Chem. B 103 (1999) 10627–10631, https://doi.org/10.1021/jp992186y.

[74] G. Vigee, J. Selbin, Proton NMR evidence for π-bonding in oxovanadium(IV) complexes, J. Inorg. Nucl. Chem. 30 (1968) 2273–2277, https://doi.org/10.1016/0022-1902(68)80230-1.

[75] C.J. Ballhausen, H.B. Gray, The Electronic Structure of the Vanadyl Ion, Inorg. Chem. 1 (1962) 111–122, https://doi.org/10.1021/ic50001a022.

[76] S.C. Larsen, DFT calculations of proton hyperfine coupling constants for [VO(H2O)5]2+: comparison with proton ENDOR data, Chem. A Eur. J. 105 (2001) 8333–8338, https://doi.org/10.1021/jp0116003.

[77] J.O. Bockris, A.K.N. Reddy, Modern Electrochemistry 1: Ionics, Springer US, Boston, MA, 1998. https://doi.org/10.1007/b114546.

[78] M.Y. Kiriukhin, K.D. Collins, Dynamic hydration numbers for biologically important ions, Biophys. Chem. 99 (2002) 155–168, https://doi.org/10.1016/S0301-4622(02)00153-9.

[79] J. Reuben, D. Fiat, Magnetic resonance studies of ion solvation. The hydration of the vanadyl(IV) ion, Inorg. Chem. 6 (1967) 579–583. https://doi.org/10.1021/ic50049a034.

[80] J. Reuben, D. Fiat, Ligand nuclear hyperfine coupling constants in the vanadyl (IV)-aquo complex. Evidence for metal-ligand .pi. bonding, Inorg. Chem. 8 (1969) 1821–1824. https://doi.org/10.1021/ic50079a003.

[81] X. Wang, A. Balwani, M. Tyagi, E.M. Davis, Capturing hydrated vanadium ion dynamics in ionomer nanocomposites used for redox flow batteries, J. Phys. Chem. B 128 (2024) 5766–5780, https://doi.org/10.1021/acs.jpcb.4c01203.

[82] V.I. Volkov, A.V. Chernyak, O.I. Gnezdilov, V.D. Skirda, Hydration, self-diffusion and ionic conductivity of Li+, Na+ and Cs+ cations in Nafion membrane studied by NMR, Solid State Ion. 364 (2021) 115627, https://doi.org/10.1016/j.ssi.2021.115627.

[83] T. Tran, C. Lin, S. Chaurasia, H. Lin, Elucidating the relationship between states of water and ion transport properties in hydrated polymers, J. Membr. Sci. 574 (2019) 299–308, https://doi.org/10.1016/j.memsci.2018.12.059.

[84] Determination of bound water content in polymers by DTA, DSC and TG, Thermochim. Acta 123 (1988) 153–161. https://doi.org/10.1016/0040-6031(88)80018-2.

[85] States of water in different hydrophilic polymers—DSC and FTIR studies, Polymer 42 (2001) 8461–8467. https://doi.org/10.1016/S0032-3861(01)00358-5.

[86] A.L. Frischknecht, B.A. Paren, L.R. Middleton, J.P. Koski, J.D. Tarver, M. Tyagi, C. L. Soles, K.I. Winey, Chain and ion dynamics in precise polyethylene ionomers, Macromolecules 52 (2019) 7939–7950, https://doi.org/10.1021/acs.macromol.9b01712.

[87] G. Schwaab, F. Sebastiani, M. Havenith, Ion hydration and ion pairing as probed by THz spectroscopy, Angew. Chem. Int. Ed. 58 (2019) 3000–3013, https://doi.org/10.1002/anie.201805261.

[88] G. Hefter, R. Buchner, Dielectric relaxation spectroscopy: an old-but-new technique for the investigation of electrolyte solutions, Pure Appl. Chem. 92 (2020) 1595–1609, https://doi.org/10.1515/pac-2019-1011.

[89] K. Wuethrich, R.E. Connick, Nuclear magnetic resonance relaxation of oxygen-17 in aqueous solutions of vanadyl perchlorate and the rate of elimination of water molecules from the first coordination sphere, Inorg. Chem. 6 (1967) 583–590, https://doi.org/10.1021/ic50049a035.

[90] L. Helm, A.E. Merbach, Water exchange on metal ions: experiments and simulations, Coord. Chem. Rev. 187 (1999) 151–181, https://doi.org/10.1016/S0010-8545(99)90232-1.

[91] S.J. Paddison, First principles modeling of sulfonic acid based ionomer membranes, in: Handbook of Fuel Cells, John Wiley & Sons Ltd, 2010, https://doi.org/10.1002/9780470974001.f303035.

[92] J. Zhu, Z. Zhang, S. Zhao, A.S. Westover, I. Belharouak, P. Cao, Single-ion conducting polymer electrolytes for solid-state lithium-metal batteries: design, performance, and challenges, Adv. Energy Mater. 11 (2021) 2003836, https://doi.org/10.1002/aenm.202003836.

[93] K. Deng, Q. Zeng, D. Wang, Z. Liu, Z. Qiu, Y. Zhang, M. Xiao, Y. Meng, Single-ion conducting gel polymer electrolytes: design, preparation and application, J. Mater. Chem. A 8 (2020) 1557–1577, https://doi.org/10.1039/C9TA11178F.

[94] K.-J. Lin, K. Li, J.K. Maranas, Differences between polymer/salt and single ion conductor solid polymer electrolytes, RSC Adv. 3 (2013) 1564–1571, https://doi.org/10.1039/C2RA21644B.

[95] M. Kanduč, W.K. Kim, R. Roa, J. Dzubiella, Selective molecular transport in thermoresponsive polymer membranes: role of nanoscale hydration and fluctuations, Macromolecules 51 (2018) 4853–4864, https://doi.org/10.1021/acs.macromol.8b00735.

[96] H.J. Cassady, E.C. Cimino, M. Kumar, M.A. Hickner, Specific ion effects on the permselectivity of sulfonated poly(ether sulfone) cation exchange membranes, J. Membr. Sci. 508 (2016) 146–152, https://doi.org/10.1016/j.memsci.2016.02.048.

[97] G.E. Boyd, B.A. Soldano, Self-diffusion of cations in and through sulfonated polystyrene cation-exchange polymers1, J. Am. Chem. Soc. 75 (1953) 6091–6099, https://doi.org/10.1021/ja01120a001.

[98] W.T. Grubb, Ionic migration in ion-exchange membranes, J. Phys. Chem. 63 (1959) 55–58, https://doi.org/10.1021/j150571a015.

[99] A. Despić, G.J. Hills, Ionic self-diffusion coefficients in ion-exchange resins, Trans. Faraday Soc. 53 (1957) 1262–1268, https://doi.org/10.1039/TF9575301262.

[100] H.P. Gregor, D. Nobel, M.H. Gottlieb, Studies on ion exchange resins. XII. Swelling in mixed solvents, J. Phys. Chem. 59 (1955) 10–13, https://doi.org/10.1021/j150523a004.

[101] H. Matsumoto, R. Yamamoto, A. Tanioka, Membrane potential across low-water-content charged membranes: effect of ion pairing, J. Phys. Chem. B 109 (2005) 14130–14136, https://doi.org/10.1021/jp051585s.

[102] R. Yamamoto, H. Matsumoto, A. Tanioka, Membrane potentials across cation-exchange membranes with a low water content, J. Phys. Chem. B 107 (2003) 10506–10512, https://doi.org/10.1021/jp0342273.

[103] S. Mafé, P. Ramírez, A. Tanioka, J. Pellicer, Model for counterion-membrane-fixed ion pairing and Donnan equilibrium in charged membranes, J. Phys. Chem. B 101 (1997) 1851–1856, https://doi.org/10.1021/jp962601b.

[104] N. Marioni, Z. Zhang, E.S. Zofchak, H.S. Sachar, S. Kadulkar, B.D. Freeman, V. Ganesan, Impact of ion-ion correlated motion on salt transport in solvated ion exchange membranes, ACS Macro Lett. 11 (2022) 1258–1264, https://doi.org/10.1021/acsmacrolett.2c00361.

[105] J.S. Mackie, P. Meares, The diffusion of electrolytes in a cation-exchange resin membrane. I. Theoretical, Proc. R. Soc. London Ser. A 232 (1955) 498–509.

[106] J.S. Mackie, P. Meares, The diffusion of electrolytes in a cation-exchange resin membrane. II. Experimental, Proc. R. Soc. London Ser. A 232 (1955) 510–518.

[107] I. Shefer, K. Lopez, A.P. Straub, R. Epsztein, Applying transition-state theory to explore transport and selectivity in salt-rejecting membranes: a critical review, Environ. Sci. Tech. 56 (2022) 7467–7483, https://doi.org/10.1021/acs.est.2c00912.

[108] S. Mafé, J.A. Manzanares, P. Ramirez, Modeling of surface vs. bulk ionic conductivity in fixed charge membranes, PCCP 5 (2003) 376–383, https://doi.org/10.1039/B209438J.

[109] S. Faucher, N. Aluru, M.Z. Bazant, D. Blankschtein, A.H. Brozena, J. Cumings, J. Pedro de Souza, M. Elimelech, R. Epsztein, J.T. Fourkas, A.G. Rajan, H.J. Kulik, A. Levy, A. Majumdar, C. Martin, M. McEldrew, R.P. Misra, A. Noy, T.A. Pham, M. Reed, E. Schwegler, Z. Siwy, Y. Wang, M. Strano, Critical knowledge gaps in mass transport through single-digit nanopores: a review and perspective, J. Phys. Chem. C 123 (2019) 21309–21326, https://doi.org/10.1021/acs.jpcc.9b02178.

[110] B.A. Soldano, G.E. Boyd, Self-diffusion of cations in hetero-ionic cation exchangers, J. Am. Chem. Soc. 75 (1953) 6107–6110, https://doi.org/10.1021/ja01120a004.